Synthesis of CdS thin films at room temperature by RF-magnetron sputtering and study of its structural, electrical, optical and morphology properties

Sachin Rondiya, Avinash Rokade, Adinath Funde, Moses Kartha, Habib Pathan, Sandesh Jadkar

PII: S0040-6090(17)30261-4
DOI: doi: 10.1016/j.tsf.2017.04.006
Reference: TSF 35914

To appear in: *Thin Solid Films*

Received date: 21 June 2016
Revised date: 2 April 2017
Accepted date: 4 April 2017

Please cite this article as: Sachin Rondiya, Avinash Rokade, Adinath Funde, Moses Kartha, Habib Pathan, Sandesh Jadkar , Synthesis of CdS thin films at room temperature by RF-magnetron sputtering and study of its structural, electrical, optical and morphology properties. The address for the corresponding author was captured as affiliation for all authors. Please check if appropriate. Tsf(2017), doi: 10.1016/j.tsf.2017.04.006

Synthesis of CdS Thin Films at Room Temperature by RF-Magnetron Sputtering and Study of its Structural, Electrical, Optical and Morphology Properties

Sachin Rondiya, Avinash Rokade, Adinath Funde

School of Energy Studies, Savitribai Phule Pune University, Pune 411 007 **(India)**

Moses Kartha, Habib Pathan, Sandesh Jadkar*

Department of Physics, Savitribai Phule Pune University, Pune 411007 **(India)**

***Corresponding author**

E-mail: sandesh@physics.unipune.ac.in **Tele:** + 91 020 2569 2678 **Fax:** + 91 020 2569 1684

ABSTRACT

Thin films of cadmium sulfide (CdS) have been deposited at room temperature by using RF-magnetron sputtering at various deposition times. Films were systematically investigated using variety of techniques such as low angle XRD, UV-Visible spectroscopy, Raman spectroscopy, x-ray photoelectron spectroscopy (XPS), scanning electron microscopy (SEM), energy-dispersive x-ray spectroscopy (EDAX), atomic force microscopy (AFM), transmission electron microscopy (TEM), four probe Van der Pauw method etc. Low angle XRD and TEM analysis revealed that films are polycrystalline having constant average crystalline size. EDAX revealed the formation of nearly stoichiometric CdS films. Surface morphology of CdS films examined using SEM shows the formation of smooth, continuous and dense films without defects such as cracks, pinholes, and protrusion. RMS roughness estimated using AFM increases with increase in deposition time. The optical studies showed decrease in band gap with increase in deposition time. The photodetector fabricated using RF sputtered CdS film show an excellent photo-response. Estimated value of growth exponent β was found ~ 0.53 which suggests uncorrelated growth of CdS films by RF sputtering. The uncorrelated growth of CdS was further confirmed by Monte-Carlo simulation.

KEYWORDS:

Semiconductors; Thin films; Transmission electron microscopy (TEM), X-ray diffraction; Scanning electron microscopy (SEM).

1: INTRODUCTION

Cadmium Sulphide (CdS) is an n-type semiconductor belonging to II-VI group of compounds which has been used in making hetero-junction thin solar cells. CdS is preferred because it is a wide band gap semiconductor having good thermal stability and can be used as light dependent resistors sensitive to visible and near infrared light. When combined with a p-type semiconductor it forms the core component of a photovoltaic solar cell. Due to wide band gap (E_g = 2.4 eV) it has been used as the window material together with several semiconductors such as CdTe [1], Cu_2S [2], InP [3] and $CuInSe_2$ [4] etc. and obtained maximum conversion efficiency ~ 14-16 % [5]. In addition CdS has been successfully employed in chemical sensor [6], surface acoustic wave devices [7] and photo-anode films of solar cells [8], thin film transistors (TFT), photocatalysis and biological sensors [9], optical coding, optical data storage and sensing [10], non-linear integrated optical devices [11].

For the deposition of CdS thin films both gas phase and liquid phase methods have been used. Gas phase method includes vacuum evaporation [12], flash evaporation [13], molecular beam epitaxy (MBE) [14], sputtering [15] and screen printing [16], pulsed laser ablation (PLA) [17] whereas liquid phase method includes electrodeposition [18], successive ionic layer adsorption and reaction (SILAR) [19], chemical bath deposition (CBD) [20], chemical spray pyrolysis (CSP) [21] etc. Each deposition method has its own advantages and limitations. Among these, RF magnetron sputtering has received considerable attention in recent years owing to its capability to synthesize CdS thin films. It permit deposition at low substrate temperature, gives better adhesion, larger coverage, high uniformity, controllable thickness, high surface mobility in condensing particles, conformal film morphologies and higher film density than other methods.

The physical properties of CdS thin films deposited by RF sputtering method are affected by deposition parameters such as sputtering power, argon gas pressure, substrate temperature, target-substrate-distance etc. These studies are based on the understanding the influence of only one of these sputter parameters on CdS thin films. However, there is lot of room for the improvement of film properties since the relation between the variation of deposition parameter and the resulting film properties has not been fully elucidated yet. In this paper, we present the detail investigation of influence of deposition time on compositional, structural, optical, morphology and electrical properties of CdS thin films deposited by RF sputtering method. Furthermore, it is important for theoretical and experimental researchers in material science to understand the growth mechanism governing the formation of material structures during

deposition process. Understanding the surface evolution of a growing film in deposition is also a subject of technological importance. Different statistical models have been proposed for the growth of CdS thin films such as random deposition (RD) [22], ballistic deposition (BD) [23], the Eden model (EM) [24], Kinetic solid-on-solid (SOS) model [25], Cluster statistical model [26], Terrace statistical model [27] etc. Here, we report experimental evidence of uncorrelated growth of CdS thin films by RF sputtering at room temperature.

2: EXPERIMENTAL DETAILS

2.1: Film preparation

Thin films of CdS were deposited on corning #7507 substrates using in-house designed locally fabricated RF-magnetron sputtering system details of which been described elsewhere [28]. It consists of a cylindrical stainless steel chamber (process chamber) coupled with a turbo molecular pump (TMP) followed by a roughing pump which yields a base pressure less than 10^{-7} Torr. A target of 4 inch diameter (99.99 % pure, Vin Karola Instrument, USA) was used for the deposition of CdS films and was kept facing the substrate holder ~ 7 cm away. In order to make the film uniformity, the substrates were kept rotating during the sputtering process using a stepper motor with variable speed. The deposition time was varied from 5 min to 25 min in steps of 5 min. The substrates can be clamped on substrate holder which is heated by inbuilt heater using thermocouple and temperature controller. The pressure during deposition was kept constant by using automated throttle valve and measured with capacitance manometer. Sputtering and reaction gases can be introduced in the process chamber through a specially designed gas bank assembly which consist of mass flow controllers (MFCs) and gas mixing. The process parameters employed during the deposition of CdS thin films are listed in Table 1.

Table 1: Process parameters employed during the deposition of CdS thin films

Process parameter	Value
Deposition Pressure	3.2×10^{-3} mBar
Deposition Time	5-25 min
RF Power	175 Watt
Distance between substrate holder and target electrode	7 cm
Ar gas flow rate	30 sccm
Substrate temperature	25 ^{0}C

The substrates were cleaned using a standard cleaning procedure. Prior to each deposition, the substrate holder and deposition chamber were baked for two hours at 100 ^{0}C in vacuum to remove any

water vapor absorbed on the substrates and to reduce the oxygen contamination in the film. Sputter-etch of 10 min were used to remove the target surface contamination. The deposition was carried out for desired amount of time and films were allowed to cool to room temperature in vacuum.

2.2: Film characterization

The electrical resistivity of CdS thin films were measured using four point probe technique in Van der Pauw geometry and photoresponce of CdS thin films were measured using two point probe method. The measurements were carried out at room temperature and atmospheric pressure. Low angle X-ray diffraction pattern were obtained by X-ray diffractometer (Bruker D8 Advance, Germany) using CuKα line (λ = 1.54056 Å). The average crystallite size was estimated using the classical Scherrer's formula [29]. The surface morphology of the films is investigated using scanning electron microscopy (JEOL JSM-6360 A). The surface topology of the films was investigated using non-contact mode atomic force microscopy (NC-AFM) (JEOL, JSPM-5200). The band gap of the films was deduced from transmittance and reflectance spectra of the films deposited on corning glass and were measured using a JASCO, V-670 UV-Visible spectrophotometer in the range 300-800 nm by using the procedure followed by Tauc [30]. Raman spectra were recorded with Raman spectroscope (Renishaw, inVia Raman Microscope) in the range 200-800 cm^{-1}. The spectrometer has backscattering geometry for detection of Raman spectrum with the resolution of 1 cm^{-1}. The excitation source was 632.8 nm line of He-Ne laser. The power of the Raman laser was kept less than 5 mW to avoid laser induced crystallization on the films. The XPS studies were carried out using VSW ESCA machine, having vacuum $>10^{-9}$ Torr, with AlKα (1486.6 eV) radiation with resolution of 1 eV. The XPS signal was obtained after several scans in the acquisition process. The spectra were recorded for all the elements as well as for specific elements. The thickness of films was determined by profilometer (KLA Tencor, P-16+) and further confirmed by UV-Visible spectroscopy analysis using the method proposed by *Swanepoel* [31].

3: RESULTS AND DISCUSSION

Sputtering is a physical vapor deposition (PVD) process in which particles are ejected from a solid target material due to bombardment of energetic particles. It only happens when the kinetic energy of the incoming particles is much higher than conventional thermal energies (≫ 1 eV). Physical sputtering is driven by momentum exchange between the ions and atoms in the target material, due to collisions [32]. Voltage is placed between the target and substrate which ionizes argon atoms and creates plasma.

These Argon ions are charged and are accelerated towards cathode (CdS target). The strong magnetic field causes electrons to travel in spiral path along magnetic flux lines near the CdS target instead of being attracted toward the substrate. It confines dense plasma near the CdS target. Also, electrons have to travel for a longer distance which increases further the probability of ionizing argon atoms. It tends to generate stable plasma with high density of ions and increases the efficiency of CdS sputtering process.

3.1: Variation in film thickness

Variation of film thickness of CdS films as a function of deposition time is shown in figure 1. As expected, the film thickness of CdS increases monotonically with increase in deposition time. It increases from 251 nm to 1285 nm when deposition time increased from 5 min to 25 min. Increase in film thickness with increase in deposition time has been reported for RF magnetron sputtered CdTe films [33].

3.2: X-ray diffraction analysis

Figure 2 display low angle XRD pattern of CdS films deposited using RF sputtering at various deposition time. Multiple diffraction peaks shows the polycrystalline nature of the deposited CdS thin films. As seen from the figure main diffraction peaks were observed at 24.67^o, 26.36^o, 28.25^o, and 43.47^o corresponding to (100), (002), (101) and (110) crystal orientations. These peaks are in agreement with JCPDS data file # 41-1049 [34].

The average grain ($d_{x\text{-}ray}$) size has been estimated using the classical *Scherrer's* formula [29],

$$d_{x\text{-}ray} = \frac{0.9\lambda}{\beta \cos\theta_\beta} \qquad \text{.....(1)}$$

Where λ is the wavelength of the x-ray used, β is full-width at half-maximum (FWHM) and θ is the Bragg diffraction angle. The average crystallite size of CdS thin films is almost constant (~ 16.70 nm) suggesting that the deposition time does not affect the crystallite size of CdS thin films.

Dislocations are an imperfection in a crystal associated with the lattice in one part with respect to another part of the crystal. The dislocation density (δ_{hkl}), defined as the length of dislocation lines per unit volume of the crystal and are given by the Williamson and Smallman's relation [35],

$$\delta = \frac{1}{d_{x\text{-}ray}} \qquad \text{.....(2)}$$

The small values of δ indicate the good crystallinity of the CdS films. The lattice strain (microstrain) which is related to misfit depends upon the growing conditions of the films. The average microstrain (ε) developed in CdS films can be calculated by using the relation [36],

$$\varepsilon = \frac{\beta \cot\theta}{4} \quad \text{.....(3)}$$

The differences in thermal expansion coefficients and lattice constants between the film and the substrate causes mechanical stress, resulting in film instability or even peeling [37]. However, no peeling of film have been observed over the entire range of deposition time studied suggesting synthesized CdS films are highly stable.

It has been observed that the estimated values for crystallite size ($d_{x\text{-}ray}$), microstrain (ϵ_{hkl}) and dislocation density (δ_{hkl}) for CdS films were ~ 16.7 nm, ~ $2.13X10^{-3}$ and ~ $3.78x10^{15}$ line/m^2 respectively over the entire range of deposition time studied. The inter-planar spacing (d) was found ~ 0.35 nm which is consistent with TEM analysis (discussed later).

3.3: Raman spectroscopy analysis

Raman spectroscopy is a powerful characterization tools to investigate molecular vibration and chemical structure by interaction of laser light with the sample. It is a non-destructive technique that offers a fast and simple way to determine the phase of the CdS [38] and one can know whether the material is amorphous, crystalline or microcrystalline. Figure 3 shows Raman spectra of CdS films in the range 200-800 cm^{-1} deposited at different time duration of deposition. We observed a broad and intense shoulder at ~ 302 cm^{-1} and a weak shoulder at ~ 604 cm^{-1} in all samples which can assign to fundamental optical phonon mode (LO) and the first over tone mode (2LO) of CdS, respectively. These are in agreement with previous reports [39]. Furthermore, the Raman spectra show that the first-order LO Raman line (~ 302 cm^{-1}) which is not only broadened with increase in deposition time but also become asymmetric towards the lower frequency side compared to bulk CdS (305 cm^{-1}). The nanometer particle size causes asymmetry and frequency shift towards the lower frequency side, which has been theoretically calculated and experimentally verified [40]. The peak at ~ 396 cm^{-1} is observed previously for CdS microcrystallite-doped glass thin film by *Jerominek et al.* [41], however the origin of it remained unidentified. Therefore, Raman spectroscopy analysis further revealed the formation of nanometer sized CdS films using RF magnetron sputtering.

3.4: X-ray photoelectron spectroscopy (XPS) analysis

The elemental bonding of CdS deposited using RF-Magnetron sputtering was examined by x-ray photoelectron spectroscopy (XPS). All XPS data were analyzed after the alignment to the C 1s peak as a reference. The binding energy was corrected for specimen charging, through referencing the C 1s to

284.6 eV. Figure 4(a) shows the XPS wide scan (0-1000 eV) of RF sputtered CdS film deposited for 25 min. deposition time. The scan shows the presence of elemental cadmium (Cd), sulfur (S), oxygen (O) and carbon (C). The core level peaks corresponding to elements Cd and S can be visibly seen in the wide scan spectra. In addition, wide scan spectra also show presence of C peak and O peak at ~ 285 eV and ~ 531 eV respectively as impurities in the CdS film. These impurities have also been identified in CdS films deposited by CBD method by other workers [42, 43]. The Gaussian fitted Cd 3d scan [Figure 4(b)] exhibits two well defined peaks at ~ 405.3 and ~ 412.1 eV, which are ascribed to the Cd $3d_{5/2}$ and Cd $3d_{3/2}$ levels resulting due to spin-orbit interaction. The energy gap between the Cd $3d_{5/2}$ and Cd $3d_{3/2}$ levels was found to be 6.8 eV. Although the relative cross section of S is small in comparison to the other elements, the S peaks are sensitive to the chemical environment. Figure 4(c) shows de-convoluted S 2p spectra of CdS in the range 158-166 eV. The lower binding energy peak at 161.24 eV is indicative of metal sulfide. The spin-orbit splitting separation was allowed to vary during fitting. The binding energy value of S $2p_{3/2}$ is ~ 161.24 eV and S $2p_{1/2}$ is ~ 162.45 eV with separation of 1.21 eV. This characteristic binding energy of S $2p_{3/2}$ and S $2p_{1/2}$ of CdS agree with those reported in the literature [44-46].

3.6: Microscopy analysis

The surface morphology and topography of the as-prepared CdS thin films on corning glass substrate was examined under scanning electron microscope (SEM) and atomic force microscope (AFM). The SEM and 2-dimensional (2D) AFM images of CdS thin films deposited at different deposition time are shown in figure 5. All SEM images [Figure 5(a1, a2, a3)] shows the formation of smooth, continuous and dense films without defects such as cracks, pinholes, and protrusion. Roughness variation of CdS film surface along a line is presented in each AFM image which was scanned using Scanning Probe Image Processor (SPIP) software and are shown in figure 5(b1, b2, b3). The total scan area of the CdS thin film was 5 μm^2. It was found that the surface roughness increases with deposition time showing the enhancement in the texture of the CdS films. During the sputter deposition the roughening of the film growth is due to interplay of the uncorrelated growth of the particles, smoothing by the surface diffusion and also due to the shadowing effects. The compositional analysis of the CdS thin films was carried out using energy dispersive x-ray analysis (EDAX) technique. Table 2 summarizes the compositional analysis of EDAX data. The Cd/S ratio increases with increasing deposition time. The EDAX data reveals the Cd:S atomic ratio for all CdS thin films are ~ 1:1 which confirms the high-quality nearly stoichiometric CdS thin films.

Table 2: Composition (EDAX) data for CdS thin films

Deposition Time (t) in min	Atomic % of S	Atomic % of Cd	Cd/S
5	51.18	48.82	0.95
10	49.79	50.21	1.00
15	49.49	50.51	1.02
20	49.43	50.57	1.02
25	49.34	50.66	1.03

To confirm the formation of nanometer size CdS, transmission electron microscopy (TEM) analysis was performed. The low resolution TEM image of CdS film deposited for 25 min using RF sputtering method is shown in figure 6(a). The image exhibit randomly distributed spherical CdS nanoparticles. Figure 6(b) and figure 6(c) are high resolution TEM micrograph and selected area electron diffraction (SAED) pattern of CdS respectively. The high resolution TEM micrograph image shows that the distance between the adjacent lattice CdS planes is ~ 0.35 nm, which is consistent with the spacing of (100) plane of CdS [JCPDS data card # 41-1049]. The bright and spotty diffraction rings in the SAED pattern [Figure 6(c)] signify a high degree of crystallinity of the material. These results are agreeing with the XRD results.

3.8: Optical properties

In order to reveal the optical properties of the CdS thin films, UV-Visible-NIR spectroscopy have been used. Figure 7(a) shows the transmittance spectra of CdS thin films prepared at different deposition time in the wavelength range 300-1200 nm. As seen from the figure, the average transmittance is > 85 % over the entire range of deposition temperature studied, which is good for solar cell applications [47]. The inset shows actual photograph of CdS film deposited for the deposition time of 25 min. The transmission strongly depends on the film structure, which is determined by the preparation methods, film thickness and deposition conditions [48]. A sharp absorption edge observed in the visible region of transmittance spectra indicate good crystallinity in the CdS films and low defect density near the band edge whereas presence of interferences fringes indicates that films have smooth surface morphology. The scanning electron microscopy analysis further supports this.

In the direct transition semiconductor, the optical energy band gap (E_{opt}) and the optical absorption coefficient (α) are related by [30],

$$\alpha E)^{1/2} = B^{1/2}(E - E_{opt}) \quad \ldots.(4)$$

Where α is the absorption coefficient, B is the optical density of state andE is the photon energy. The absorption coefficient (a) can be calculated from the transmittance of the films with the formula,

$$\alpha = \frac{1}{d} \ln\left(\frac{1}{T}\right) \quad \text{.....(5)}$$

Where d is the thickness of the films and T is the transmittance. Therefore, the optical band gap is obtained by extrapolating the tangential line to the photon energy ($E = h\upsilon$) axis in the plot of $\alpha h\upsilon$ as a function of $h\upsilon$. The variation of optical band gap as a function of deposition time is shown in figure 7(b). As seen the band gap decreases from 3.08 eV to 2.47 eV when the deposition time increased from 5 min to 25 min. These values of the band gap were higher than the band gap of bulk CdS (2.42 eV) [49]. *Raghvendra et al.* [50] and *Dongre et al.* [51] have also reported high band gap values for CdS films deposited by chemical bath deposition method and sonochemical process respectively. These results suggest that high band gap makes CdS a more effective window material in photovoltaic applications like the CdS/CdTe and CdS/Cu_2S solar cells.

3.8: Electrical properties

Electrical properties of the material are utmost important in order to use it in solar cell application. The resistivity values of the different films were measured by using four probe Van der Pauw geometry. For the resistivity measurement, the four ohmic contacts were made by using indium wire at the four corners of the film sample. The sheet resistance (R_s) of a given CdS film was calculated by using,

$$2\, e^{-R/R_s} = 1 \quad \text{....(6)}$$

Where, R is the average resistance measured between four points of the film. The resistivity (ρ) of CdS film was obtained by using the following equation,

$$\rho = R_s \times t \quad \text{.....(7)}$$

Where, R_s is the sheet resistance of CdS film and t is thickness.

Figure 8 shows variation of resistivity of CdS films as a function of deposition time. As seen from the figure all films exhibited semiconductor behavior with resistivity in between 2.0 x10^4 Ω-m and 9.0x10^4 Ω-m over the entire range of deposition time studied. This high resistivity is attributed to dislocations and imperfections of the films and the results are in good agreement with the literature [52].

To demonstrate the photo response of CdS films, samples of dimension 3 cm x 1 cm deposited on glass substrate were used. The coplanar Al electrodes 0.5 mm apart were deposited on it by vacuum evaporation. A constant DC voltage was applied to the electrodes and the current was measured using a system sourcemeter (Keithley, Model 2400). The measurements were done first under dark condition, and then the specimen was illuminated by a halogen lamp, with an intensity 100 mW/cm^2,

which was calibrated using a standard c-Si solar cell. Figure 9 shows the photo-response of CdS films prepared at deposition time 25 min. As seen from the figure, the RF sputtered CdS film show excellent photo-response with the rise and decay curves. The rise and decay curves of photocurrent are governed by the trapping states and recombination centers lying in the forbidden of a photoconductor [53]. The general nature of the curve shows a rapid rise of photocurrent when the lamp is ON, which is followed by a slower decay of photocurrent when the lamp is switch OFF. The early part of rise in photocurrent is due to generation of carriers upon illumination and later slower decrease is due to recombination effect after switching off the source is related to a slow release of trapped electron from traps formed in CdS system.

3.9: Uncorrelated Growth and Monte-Carlo Simulation

Sarma et al. [54] reported that the surface roughness (w) of the film varies with the deposition time (t) showing the power law behaviour,

$$w \sim t^{\beta} \qquad .....(8)$$

Where $\beta = 0.5$ for uncorrelated or random deposition, 0.25 for growth processes dominated by surface diffusion, 0.33 for ballistic deposition and 1 is for the growth process with shadowing effects. Figure 10 represents the plot of ln(RMS roughness) estimated from AFM analysis versus ln(deposition time) of CdS films deposited using RF sputtering method. From the plot, estimated value of the growth exponent β was found to be 0.53 which suggests the uncorrelated or random growth of CdS films by RF sputtering. The average grain size ($d_{x\text{-}ray}$) obtained from XRD analysis further support this because it is well established that the average grain size remains unchanged in uncorrelated growth [55]. Figure 11 explains the uncorrelated growth mechanism of CdS thin films by using RF sputtering onto the substrate. The yellow circles (A, B, C) are CdS particles, moving towards substrate, green circles (A', B', C') represent the sites of CdS atoms which are allowed in random deposition model and red circles (A", B", C") represent forbidden deposition sites.

Further to support the formation of CdS films by uncorrelated growth mechanism we have carried out the Monte-Carlo simulation on growth of CdS films by RF magnetron sputtering. The simulations were carried out for 10^4 time steps and all the roughness values are obtained by averaging over 100 configurations. The depositing time (t) is defined as number of the launched particles mimicking the process having the uniform flux. The number of launched particles mimicking the process was kept at lattice size (L) = 128. We choose a column i randomly and increase its height h(i, t) by one for every deposition. The interface width (ω) was calculated using relation [56],

$$\omega(L,t) = \sqrt{\frac{1}{L}\sum_{i=1}^{L}\left[h(i,\ t) - \bar{h}\right]^2} \qquad .....(9)$$

Where, h(i, t) is the surface height at the time t and $\bar{h}$ is the average height of the surface at the time t. Figure 12 shows the typical interface of the uncorrelated growth model under the Monte-Carlo simulation. The different colors indicate the interface after every 100 steps. The figure 12 depicts the interface configuration for 5 sets with 100 time steps each. As seen the interface roughness increases with increase in deposition time and all columns grow independently, as there is no mechanism that can generate correlations along the lateral interface. Thus, Monte-Carlo simulation results further confirm the formation of CdS films in RF sputtering method by uncorrelated growth mechanism.

4: CONCLUSIONS

Cadmium sulfide (CdS) thin films have been deposited on glass substrates at room temperature using RF sputtering at various deposition times. It was found that thickness of the films increases with increase in deposition time. Low angle XRD and TEM revealed that films are polycrystalline with constant average crystalline size over the entire range of deposition time studied. The EDAX analysis revealed the formation of nearly stoichiometric CdS films. Formation of CdS films were also confirmed by Raman spectroscopy and XPS. Surface morphology of CdS thin films examined using SEM shows the formation of smooth, continuous and dense films without defects such as cracks, pinholes, and protrusion. The RMS roughness estimated using AFM increases with increase in deposition time. Optical studies showed that with increase in deposition time, the band gap decreases from 3.08 eV to 2.47 eV. Electrical measurements show increase in electrical resistivity with increase in deposition time. A photodetector fabricated using RF sputtered CdS film show excellent photo-response. The estimated value of the growth exponent β was found to be 0.53 which suggests the uncorrelated growth of CdS films by RF sputtering at room temperature which is further validated by Monte-Carlo simulation.

ACKNOWLEDGEMENT:

Authors are thankful to Department of Science and Technology (DST) and Ministry of New and Renewable Energy (MNRE), Government of India, New Delhi for the financial support. Sachin Rondiya gratefully acknowledges the financial support from Dr. Babasaheb Ambedkar Research and Training Institute (BARTI), Pune, for the award of Junior Research Fellowship. Avinash Rokade is grateful to

Ministry of New and Renewable Energy (MNRE), New Delhi for National Renewable Energy (NRE) fellowship and financial assistance. Sandesh Jadkar is thankful to University Grants Commission, New Delhi for special financial support under UPE program.

REFERENCES:

[1] B. Lv, L. Ma, Y. Li, B. Yan, P. Cai, X. Wu, The phase segregation in CdTe/CdS heterojunction and its effect on photo current of CdTe thin films solar cell, Sol. Energy, 136 (2016) 460-469. http://dx.doi.org/10.1016/j.solener.2016.07.030

[2] T. Shen, L. Bian, B. Li, K. Zheng, T. Pullerits, J. Tian, A structure of CdS/CuxS quantum dots sensitized solar cells, Appl. Phys. Lett., 108 (2016) 213901. http://dx.doi.org/10.1063/1.4952435

[3] D.G. Sellers, M.F. Doty, Design, synthesis and photophysical properties of InP/CdS/CdSe and CdTe/CdS/CdSe (core/shell/shell) quantum dots for photon upconversion, Photovoltaic Specialist Conference (PVSC), IEEE 42nd, (2015) 1-5. https://doi.org/10.1109/PVSC.2015.7356445

[4] F.I. Lai, J.-F. Yang, M.-C. Lee, S.-Y. Kuo, Investigation of the copper concentration on photocurrent collection of CuInSe2 solar cells, Int. J. Energy Res., 40 (2016) 1957-1965. http://onlinelibrary.wiley.com/doi/10.1002/er.3573/full

[5] B. Su, K.L. Choy, Electrostatic assisted aerosol jet deposition of CdS, CdSe and ZnS thin films, Thin Solid Films, 361–362 (2000) 102-106. http://dx.doi.org/10.1016/S0040-6090(99)00857-3

[6] A. Apolinar-Iribe, M. Acosta-Enriquez, M. Quevedo-Lopez, R. Ramirez-Bon, A. De Leon, S. Castillo, Acetylacetone as complexing agent for CdS thin films grow chemical bath deposition, Chalcogenide Letters, 8 (2011) 77-82.http://www.chalcogen.ro/77_Apolynar-Ibre.pdf

[7] B. Wacogne, M.P. Roe, T.J. Pattinson, C.N. Pannell, Effective piezoelectric activity of zinc oxide films grown by radio-frequency planar magnetron sputtering, Appl. Phys. Lett., 67 (1995) 1674-1676. http://aip.scitation.org/doi/abs/10.1063/1.115053

[8] K. Keis, E. Magnusson, H. Lindström, S.-E. Lindquist, A. Hagfeldt, A 5 % efficient photoelectrochemical solar cell based on nanostructured ZnO electrodes, Sol. Energy Mater. Sol. Cells, 73 (2002) 51-58. http://dx.doi.org/10.1016/S0927-0248(01)00110-6

[9] P. Sharma, D.S. Rana, A. Umar, R. Kumar, M.S. Chauhan, S. Chauhan, Synthesis of cadmium sulfide nanosheets for smart photocatalytic and sensing applications, Ceram. Int., 42 (2016) 6601-6609. http://dx.doi.org/10.1016/j.ceramint.2015.12.151

[10] J. Trajic, M. Gilic, N. Romcevic, M. Romcevic, G. Stanisic, B. Hadzic, M. Petrovic, Y. Yahia, Raman Spectroscopy of Optical Properties In CdS Thin Films, Science of Sintering, 47 (2015) 145-152. doi:10.2298/SOS1502145T

[11] K. Senthil, D. Mangalaraj, S.K. Narayandass, Structural and optical properties of CdS thin films, Appl. Sur. Sci., 169–170 (2001) 476-479. http://dx.doi.org/10.1016/S0169-4332(00)00732-7

[12] K.C. Sarma, R.K. Bordoloi, M. Sarma, J.N. Ganguli, Chemical bath deposition of cadmium sulphide (CdS) thin film for optical and optoelectronic applications, J Instrum Soc India, 31 (2001) 216-221.

[13] V. Gevorgyan, L. Hakhoyan, N. Mangasaryan, P. Gladyshev, Substrate temperature and annealing effects on the structural and optical properties of nano-CdS films deposited by vacuum flash evaporation technique, Chalcogenide Letters, 13 (2016) 331-338. http://www.chalcogen.ro/331_GevorgyanV.pdf

[14] J. Shay, S. Wagner, K. Bachman, E. Buchler, HM Kasper Proc. 11th Photovoltaic Specialists' Conf., Phoenix, AZ, May 6-8, 1975, IEEE, New York, (1975) 503.

[15] J. Tao, J. Liu, L. Chen, H. Cao, X. Meng, Y. Zhang, C. Zhang, L. Sun, P. Yang, J. Chu, 7.1% efficient co-electroplated Cu_2ZnSnS_4 thin film solar cells with sputtered CdS buffer layers, Green Chem., 18 (2016) 550-557. http://pubs.rsc.org/-/content/articlehtml/2016/gc/c5gc02057c

[16] A. Giberti, D. Casotti, G. Cruciani, B. Fabbri, A. Gaiardo, V. Guidi, C. Malagù, G. Zonta, S. Gherardi, Electrical conductivity of CdS films for gas sensing: Selectivity properties to alcoholic chains, Sens., Actuators B, 207 (2015) 504-510. http://dx.doi.org/10.1016/j.snb.2014.10.054

[17] T.M. Khan, T. BiBi, Application of NS Pulsed Laser Ablation for Dense CdS Nanoparticles Deposition in Argon Atmosphere, SOP Transactions on Applied Physics, 1 (2014) 48-54.

[18] Y. Zhang, H. Ma, D. Wu, R. Li, X. Wang, Y. Wang, W. Zhu, Q. Wei, B. Du, A generalized in situ electrodeposition of Zn doped CdS-based photoelectrochemical strategy for the detection of two metal ions on the same sensing platform, Biosens. Bioelectronics, 77 (2016) 936-941. http://dx.doi.org/10.1016/j.bios.2015.10.074

[19] W. Kim, M. Baek, K. Yong, Fabrication of ZnO/CdS, ZnO/CdO core/shell nanorod arrays and investigation of their ethanol gas sensing properties, Sens., Actuators B, 223 (2016) 599-605. http://dx.doi.org/10.1016/j.snb.2015.09.158

[20] K.C. Wilson, M. Basheer Ahamed, Surface modification of cadmium sulfide thin film honey comb nanostructures: Effect of in situ tin doping using chemical bath deposition, Appl. Surf. Sci., 361 (2016) 277-282. http://dx.doi.org/10.1016/j.apsusc.2015.11.184

[21] S. Yılmaz, Y. Atasoy, M. Tomakin, E. Bacaksız, Comparative studies of CdS, CdS:Al, CdS:Na and CdS:(Al–Na) thin films prepared by spray pyrolysis, Superlattices Microstruct., 88 (2015) 299-307. http://dx.doi.org/10.1016/j.spmi.2015.09.021

[22] J. Evans, Random-deposition models for thin-film epitaxial growth, Phys. Rev. B, 39 (1989) 5655-5664. https://journals.aps.org/prb/abstract/10.1103/PhysRevB.39.5655

[23] F.A. Reis, Universality and corrections to scaling in the ballistic deposition model, Phys. Rev. E, 63 (2001) 056116-5. https://journals.aps.org/pre/abstract/10.1103/PhysRevE.63.056116

[24] R. Jullien, R. Botet, Surface thickness in the Eden model, Phys. Rev. Lett., 54 (1985) 2055. https://journals.aps.org/prl/abstract/10.1103/PhysRevLett.54.2055

[25] S.D. Sarma, P.P. Chatraphorn, Z. Toroczkai, Universality class of discrete solid-on-solid limited mobility nonequilibrium growth models for kinetic surface roughening, Phys. Rev. E, 65 (2002) 036144. https://journals.aps.org/pre/abstract/10.1103/PhysRevE.65.036144

[26] Z. Volkovich, Z. Barzily, L. Morozensky, A statistical model of cluster stability, Pattern Recognit., 41 (2008) 2174-2188. http://dx.doi.org/10.1016/j.patcog.2008.01.008

[27] C. Lent, P. Cohen, Diffraction from stepped surfaces: I. Reversible surfaces, Surf. Sci., 139 (1984) 121-154. http://dx.doi.org/10.1016/0039-6028(84)90013-X

[28] A. Jadhavar, A. Bhorde, V. Waman, A. Funde, A. Pawbake, R. Waykar, D. Patil, S. Jadkar, Synthesis of indium tin oxide (ITO) as a transparent conducting layer for solar cells by RF sputtering. Engineering Sciences International Research Journal, 3 (2015) 126-130.

[29] B. Cullity, S. Stock, Elementary of X-ray Diffraction, Englewood Cliffs, 3rd Edn. (2001).

[30] J. Tauc, A. Menth, States in the gap, J. Non-Cryst. Solids, 8 (1972) 569-585. http://dx.doi.org/10.1016/0022-3093(72)90194-9

[31] R. Swanepoel, Determination of the thickness and optical constants of amorphous silicon, J. Phys. E: Sci. Instru., 16 (1983) 1214-1222.http://iopscience.iop.org/article/10.1088/0022-3735/16/12/023/meta

[32] P. Sigmund, Mechanisms and theory of physical sputtering by particle impact, Nucl. Instru. Methods, Phys. Res., Sect. B., 27 (1987) 1-20. http://dx.doi.org/10.1016/0168-583X(87)90004-8

[33] E. Camacho-Espinosa, E. Rosendo, A. Oliva, T. Diaz, N. Carlos-Ramirez, H. Juarez, G. García, M. Pacio, Physical properties of sputtered CdTe thin films, Indian Journal of Applied Reseach, 4 (2014) 588-592. DOI : 10.15373/2249555X

[34] N. Srinivasan, S. Thirumaran, Effect of pyridine as a ligand in precursor on morphology of CdS nanoparticles, Superlattices Microstruct., 51 (2012) 912-920.http://dx.doi.org/10.1016/j.spmi.2012.03.006

[35] G. Williamson, R. Smallman, Dislocation densities in some annealed and cold-worked metals from measurements on the X-ray debye-scherrer spectrum, Journal Philosophical Magazine, 1 (1956) 34-46. http://dx.doi.org/10.1080/14786435608238074

[36] K. Girija, S. Thirumalairajan, S. Mohan, J. Chandrasekaran, Structural, morphological and optical studies of CdSe thin films from ammonia bath, Chalcogenide Letters, 6 (2009) 351-357.http://chalcogen.ro/351_Girija-aug3.pdf

[37] Y. Dingyu, Z. Xinghua, W. Zhaorong, Y. Weiqing, L. Lezhong, Y. Jun, G. Xiuying, Structural and optical properties of polycrystalline CdS thin films deposited by electron beam evaporation, J. Semi., 32 (2011) 023001(1-4).http://iopscience.iop.org/article/10.1088/1674-4926/32/2/023001/pdf

[38] D. Chuu, C. Dai, W. Hsieh, C. Tsai, Raman investigations of the surface modes of the crystallites in CdS thin films grown by pulsed laser and thermal evaporation, J. Appl. Phys., 69 (1991) 8402-8404.doi: http://dx.doi.org/10.1063/1.347405

[39] P. Kumar, N. Saxena, R. Chandra, V. Gupta, A. Agarwal, D. Kanjilal, Nanotwinning and structural phase transition in CdS quantum dots, Nanoscale Res. Lett., 7 (2012) 1-7.DOI: 10.1186/1556-276X-7-584

[40] H. Richter, Z. Wang, L. Ley, The one phonon Raman spectrum in microcrystalline silicon, Solid State Commun., 39 (1981) 625-629.http://dx.doi.org/10.1016/0038-1098(81)90337-9

[41] H. Jerominek, M. Pigeon, S. Patela, Z. Jakubczyk, C. Delisle, R. Tremblay, CdS microcrystallites-doped thin-film glass waveguides, J. Appl. Phys., 63 (1988) 957-959. doi: http://dx.doi.org/10.1063/1.340039

[42] H. El Maliki, J. Bernede, S. Marsillac, J. Pinel, X. Castel, J. Pouzet, Study of the influence of annealing on the properties of CBD-CdS thin films, Appl. Surf. Sci., 205 (2003) 65-79.http://dx.doi.org/10.1016/S0169-4332(02)01082-6

[43] P. Roy, S.K. Srivastava, A new approach towards the growth of cadmium sulphide thin film by CBD method and its characterization, Mater. Chem. Phys., 95 (2006) 235-241.http://dx.doi.org/10.1016/j.matchemphys.2005.06.010

[44] G. Hota, S. B. Idage, Kartic C. Khilar, Characterization of nano-sized CdS–Ag2S core-shell nanoparticles using XPS technique, Colloids Surf. A., 293 (2007) 5-12.http://dx.doi.org/10.1016/j.colsurfa.2006.06.036

[45] T. Rakshit, S.P. Mondal, I. Manna, S.K. Ray, CdS-decorated ZnO nanorod heterostructures for improved hybrid photovoltaic devices, ACS Appl. Mater. Interfaces, 4 (2012) 6085-6095.http://pubs.acs.org/doi/abs/10.1021/am301721h

[46] T.Y. Lee, I.H. Lee, S.H. Jung, C.W. Chung, Characteristics of CdS thin films deposited on glass and Cu (In, Ga) Se 2 layer using chemical bath deposition, Thin Solid Films, 548 (2013) 64-68. http://dx.doi.org/10.1016/j.tsf.2013.08.101

[47] A. Obaid, Z. Hassan, M. Mahdi, M. Bououdina, Fabrication and characterisations of n-CdS/p-PbS heterojunction solar cells using microwave-assisted chemical bath deposition, Sol. Energy, 89 (2013) 143-151.http://dx.doi.org/10.1016/j.solener.2012.12.010

[48] A. Pérez González, I. Arreola, C. Tepantlán, Effects of indium doping on the structural and optical properties of CdSe thin films deposited by chemical bath, Rev. Mex. Fis., 55 (2009) 51-54.http://www.scielo.org.mx/scielo.php?pid=S0035-001X2009000100007&script=sci_arttext&tlng=en

[49] J.P. Enríquez, X. Mathew, Influence of the thickness on structural, optical and electrical properties of chemical bath deposited CdS thin films, Sol. Energy Mater. Sol. Cells, 76 (2003) 313-322. http://dx.doi.org/10.1016/S0927-0248(02)00283-0

[50] P. Mishra, R.S. Yadav, A.C. Pandey, Growth mechanism and photoluminescence property of flower-like ZnO nanostructures synthesized by starch-assisted sonochemical method, Ultrason. Sonochem., 17 (2010) 560-565. http://dx.doi.org/10.1016/j.ultsonch.2009.10.017

[51] J. Dongre, V. Nogriya, M. Ramrakhiani, Structural, optical and photoelectrochemical characterization of CdS nanowire synthesized by chemical bath deposition and wet chemical etching, Appl. Surf. Sci., 255 (2009) 6115-6120. http://dx.doi.org/10.1016/j.apsusc.2009.01.064

[52] R.K. Nkum, A.A. Adimado, H. Totoe, Band gap energies of semiconducting sulphides and selenides, Materials Science and Engineering: B, 55 (1998) 102-108. http://dx.doi.org/10.1016/S0921-5107(98)00193-7

[53] P. Nair, M. Nair, A. Fernandez, M. Ocampo, Prospects of chemically deposited metal chalcogenide thin films for solar control applications, J. Phys. D: Appl. Phys., 22 (1989) 829-836. http://iopscience.iop.org/article/10.1088/0022-3727/22/6/021/meta

[54] S.D. Sarma, P. Tamborenea, A new universality class for kinetic growth: One-dimensional molecular-beam epitaxy, Phys. Rev. Lett., 66 (1991) 325-328. https://doi.org/10.1103/PhysRevLett.66.325

[55] R. Almeida, S. Ferreira, I. Ribeiro, T. Oliveira, Temperature effect on (2+ 1) experimental Kardar-Parisi-Zhang growth, Europhys. Lett., 109 (2015) 46003(1-6). http://iopscience.iop.org/article/10.1209/0295-5075/109/46003/meta

[56] A.L. Barabási, H.E. Stanley, Fractal concepts in surface growth, Cambridge university press (1995).

FIGURE CAPTIONS:

Figure 1: Variation of film thickness as a function of deposition time for CdS films prepared by RF sputtering

Figure 2: XRD pattern of CdS thin films deposited at different deposition time

Figure 3: Raman spectra of CdS thin films deposited at different deposition time

Figure 4: Typical XPS spectra for CdS film deposited at 25 minutes sputter time by RF sputtering **(a)** Wide scan in the range 0 eV-1000 eV **(b)** Cd 3d spectra in the range 398 eV-418 eV **(c)** S 2p spectra in the range 158 eV-166 eV

Figure 5: a1, a2, a3) Scanning electron microscopy (SEM) images and **b1, b2, b3)** Two dimensional (2-D) AFM scans for CdS films deposited at deposition times (t) = 5, 15, 25 min respectively.

Figure 6: a) Low resolution TEM image **b)** High resolution TEM image and **c)** Selected area electron diffraction (SAED) pattern of CdS film deposited for 25 minutes using RF sputtering method

Figure 7: a) Transmittance spectra of CdS films prepared at different deposition time. Inset shows the actual photograph of CdS film deposited for 25 min. and **b)** Variation of optical band gap as a function of deposition time

Figure 8: Variation of resistivity of CdS films as a function of deposition time

Figure 9: Photo-response of CdS films prepared at deposition time 25 min

Figure 10: Plot of ln(RMS roughness) versus ln(deposition time) of CdS films deposited using RF sputtering method

Figure 11: Growth mechanism CdS onto substrate from random deposition model

Figure 12: Typical interface configuration for 5 sets with 100 time steps each of the random deposition model under the Monte-Carlo simulation

Figure 01: Sachin Rondiya et al.

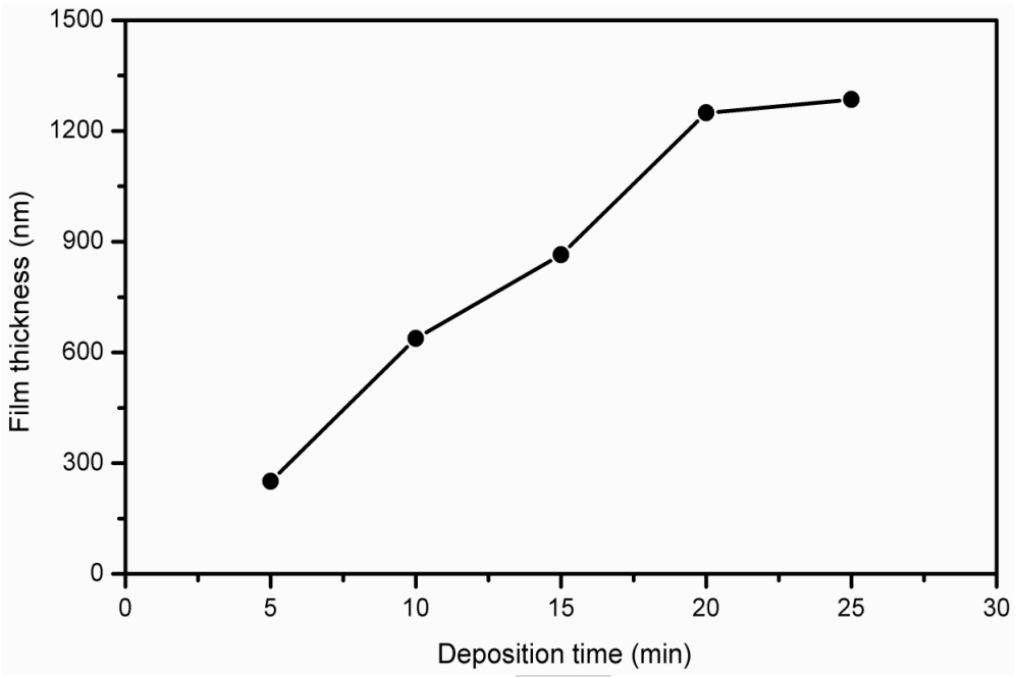

Figure 02: Sachin Rondiya et al.

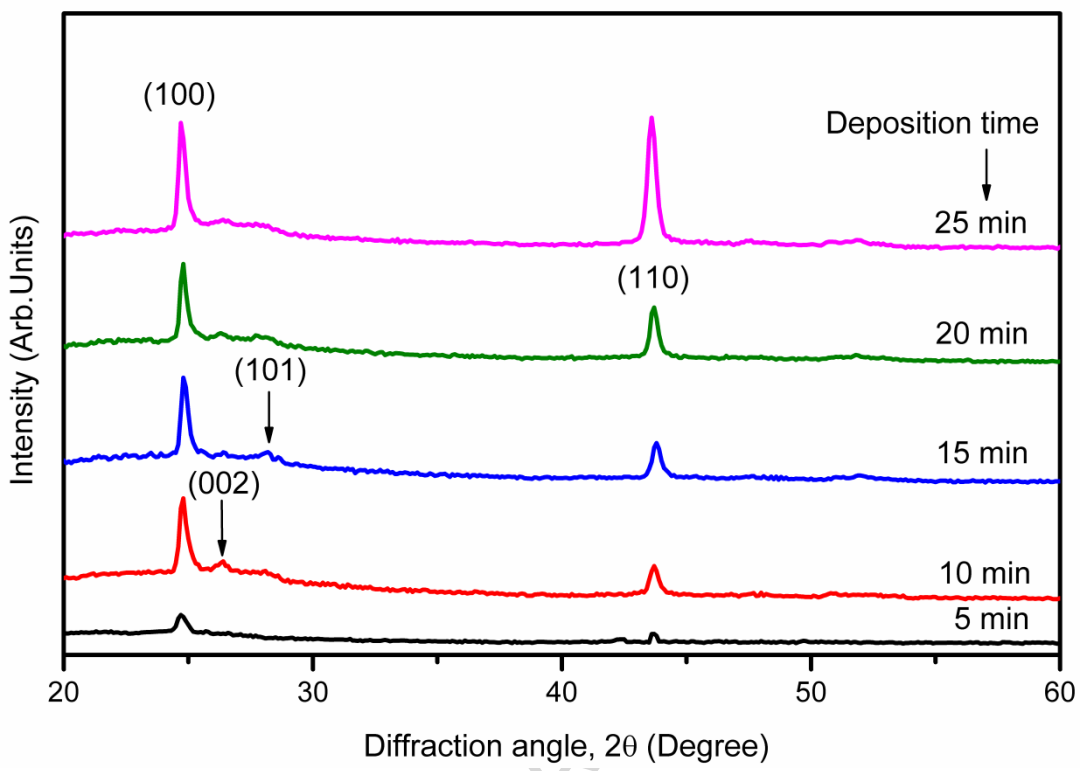

Figure 03: Sachin Rondiya et al.

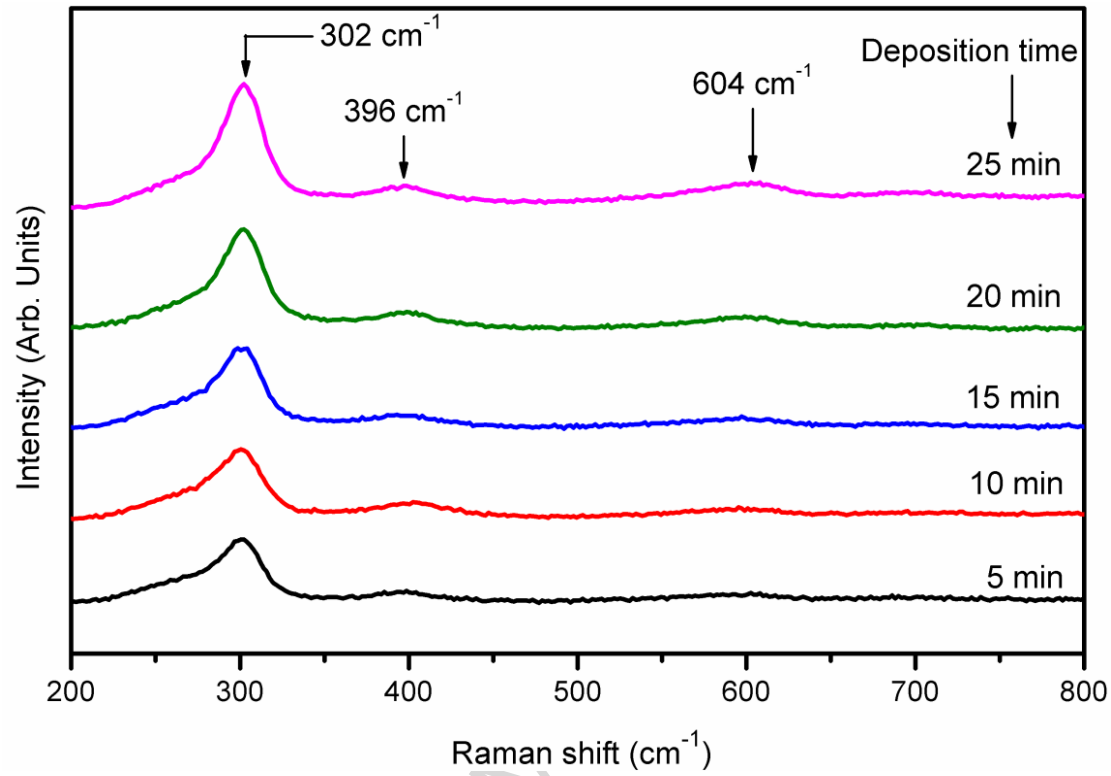

Figure 04: Sachin Rondiya et al.

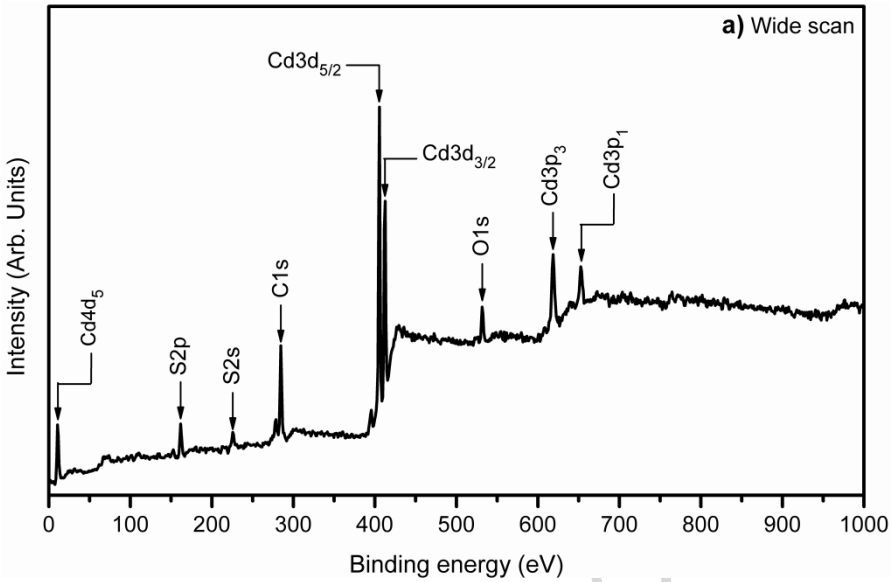

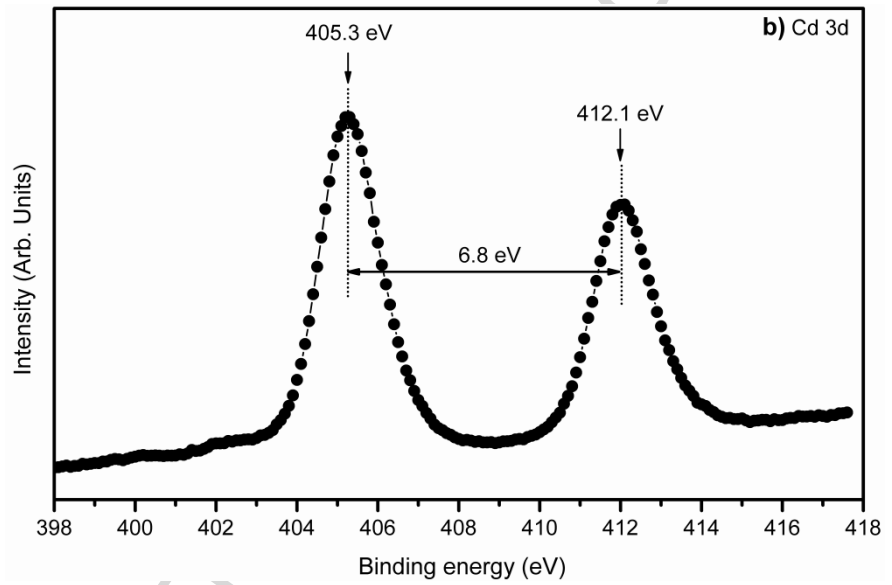

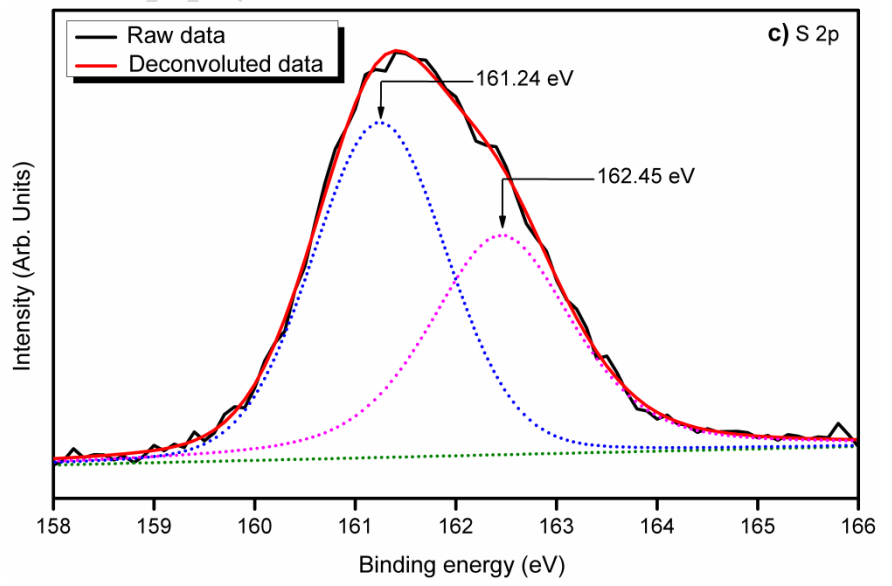

Figure 05: Sachin Rondiya et al.

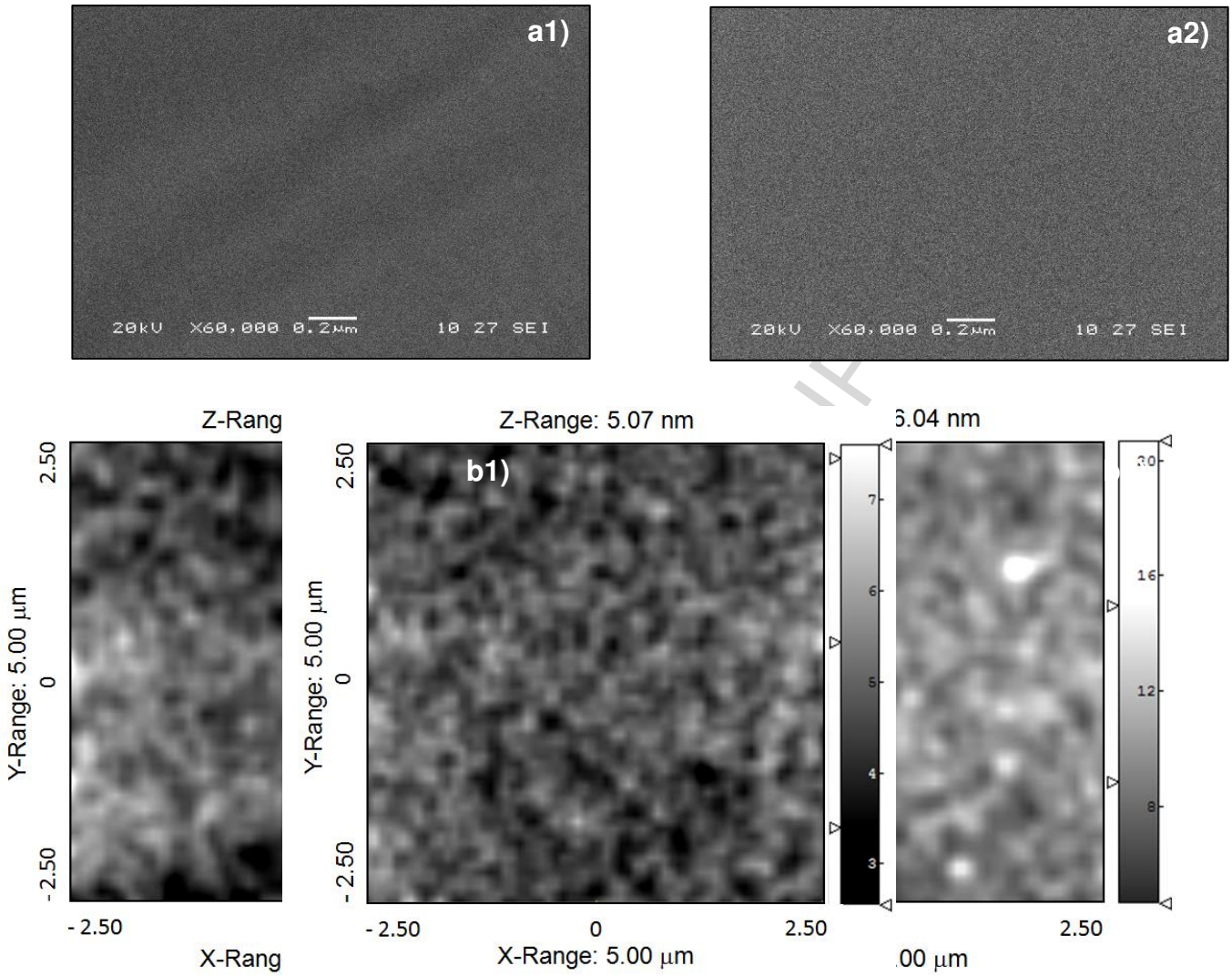

Figure 06: Sachin Rondiya et al.

.

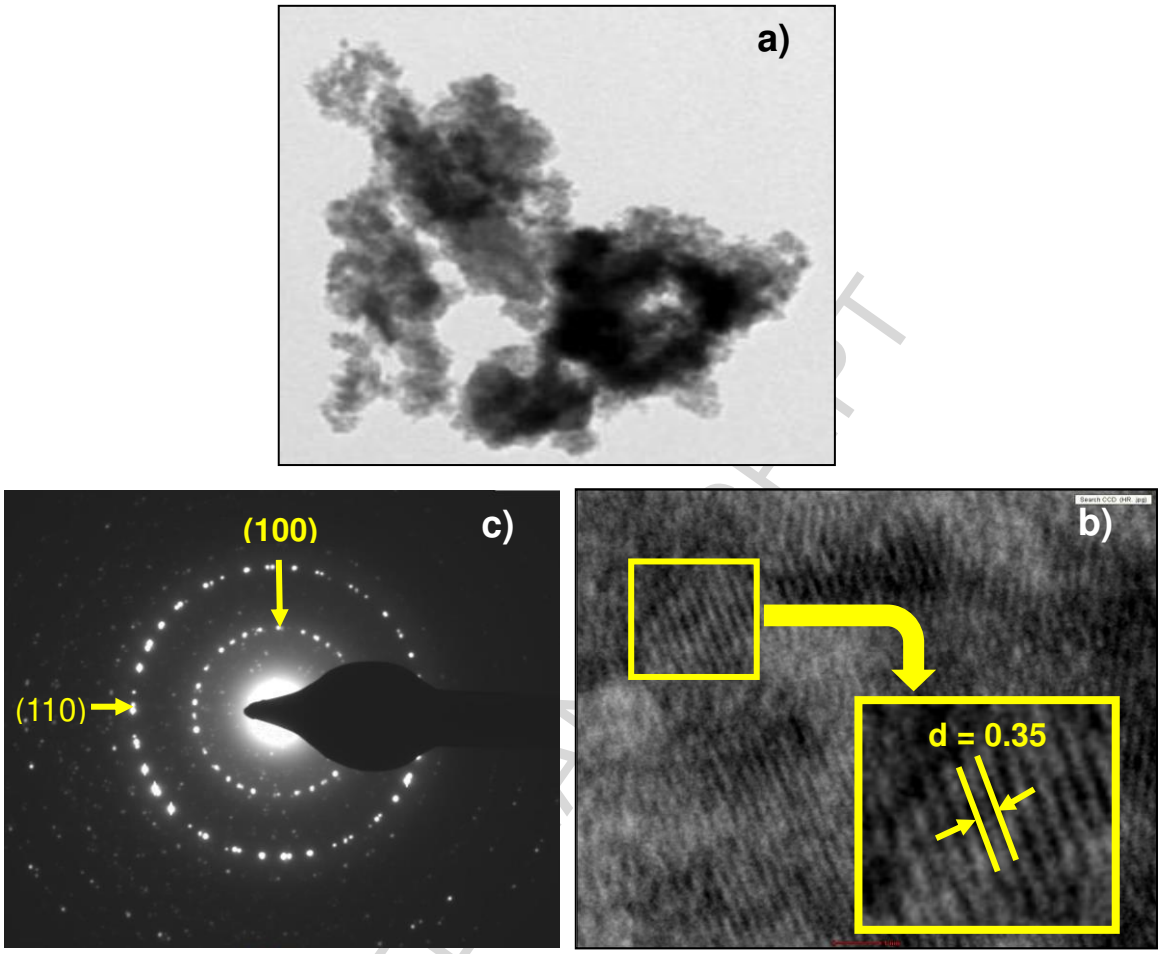

Figure 07: Sachin Rondiya et al.

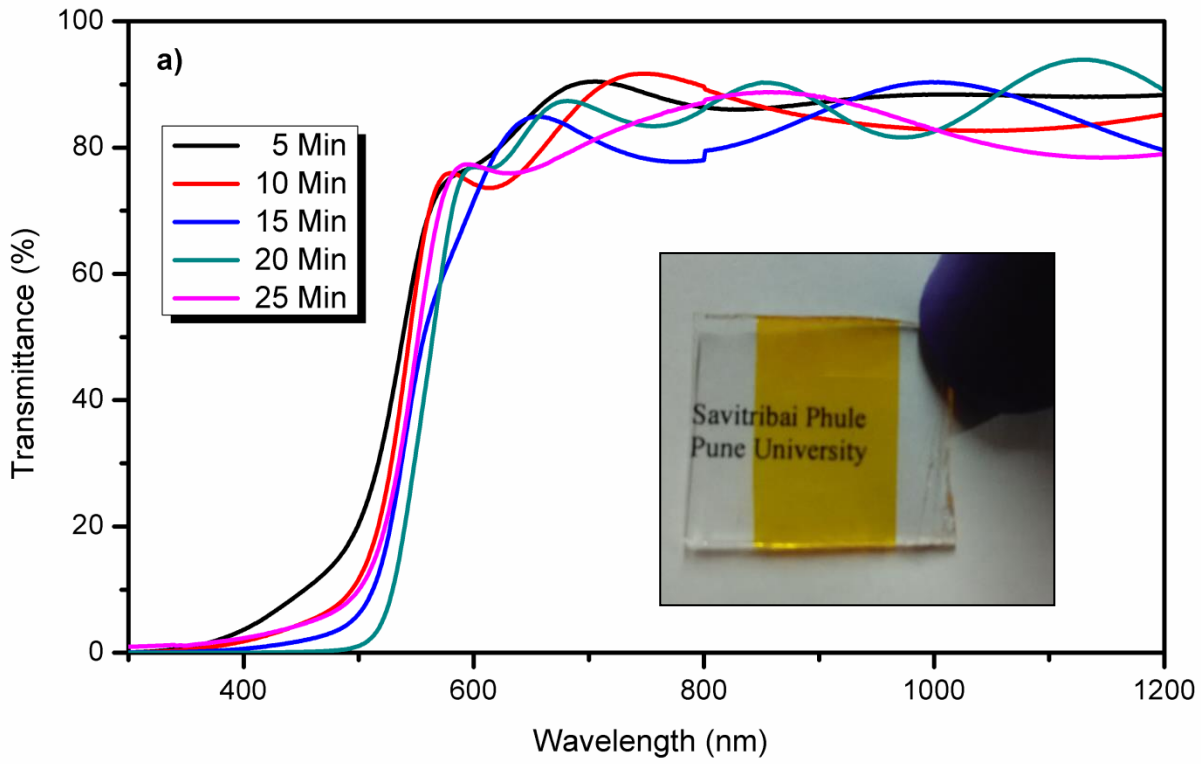

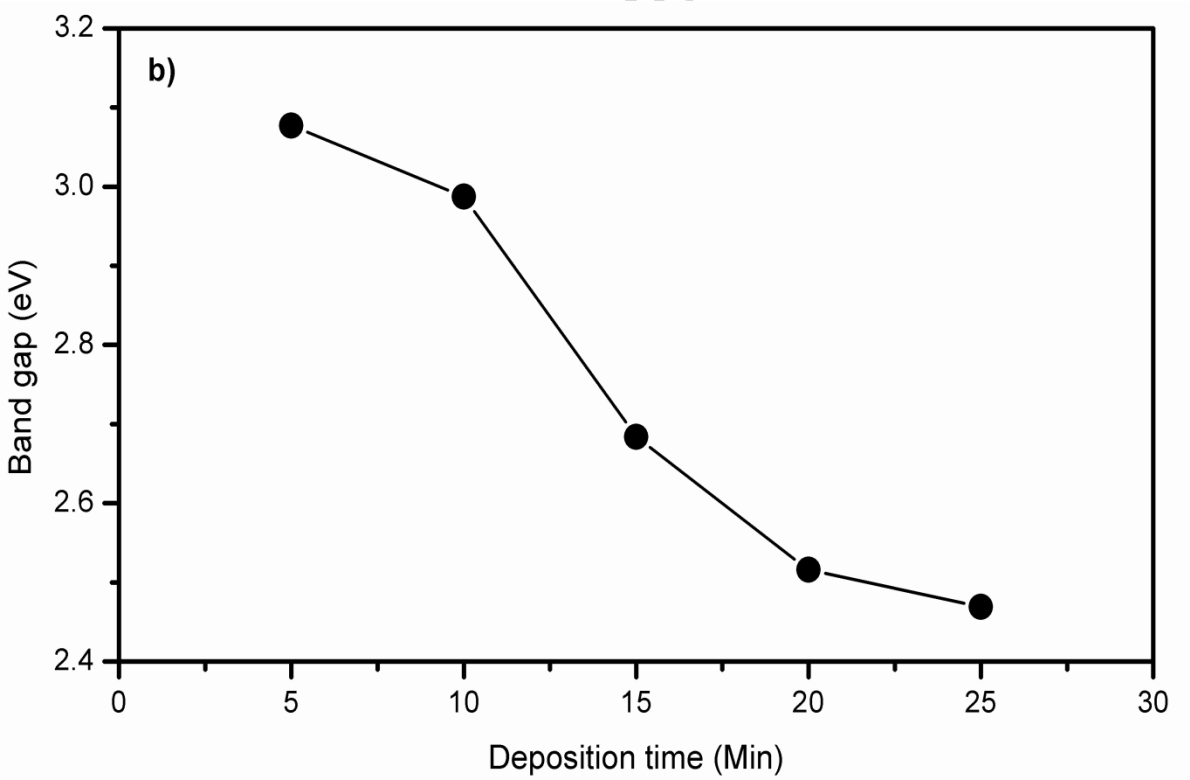

Figure 08: Sachin Rondiya et al.

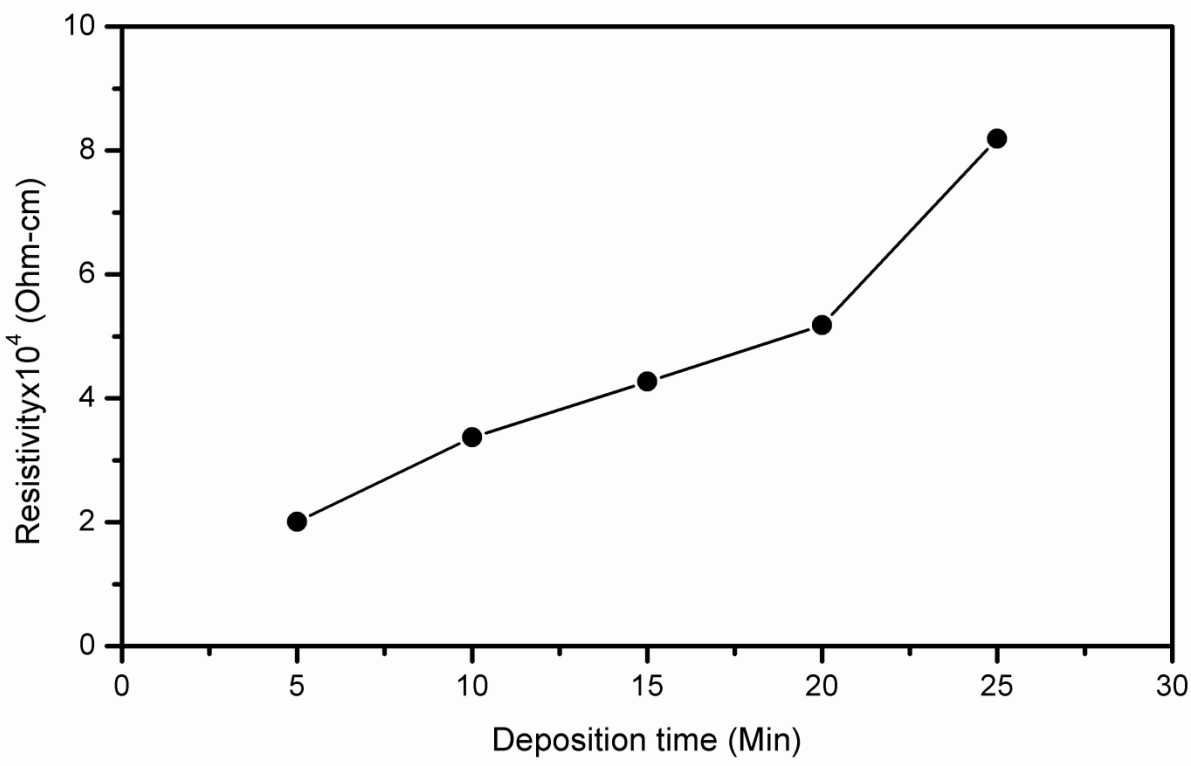

Figure 09: Sachin Rondiya et al.

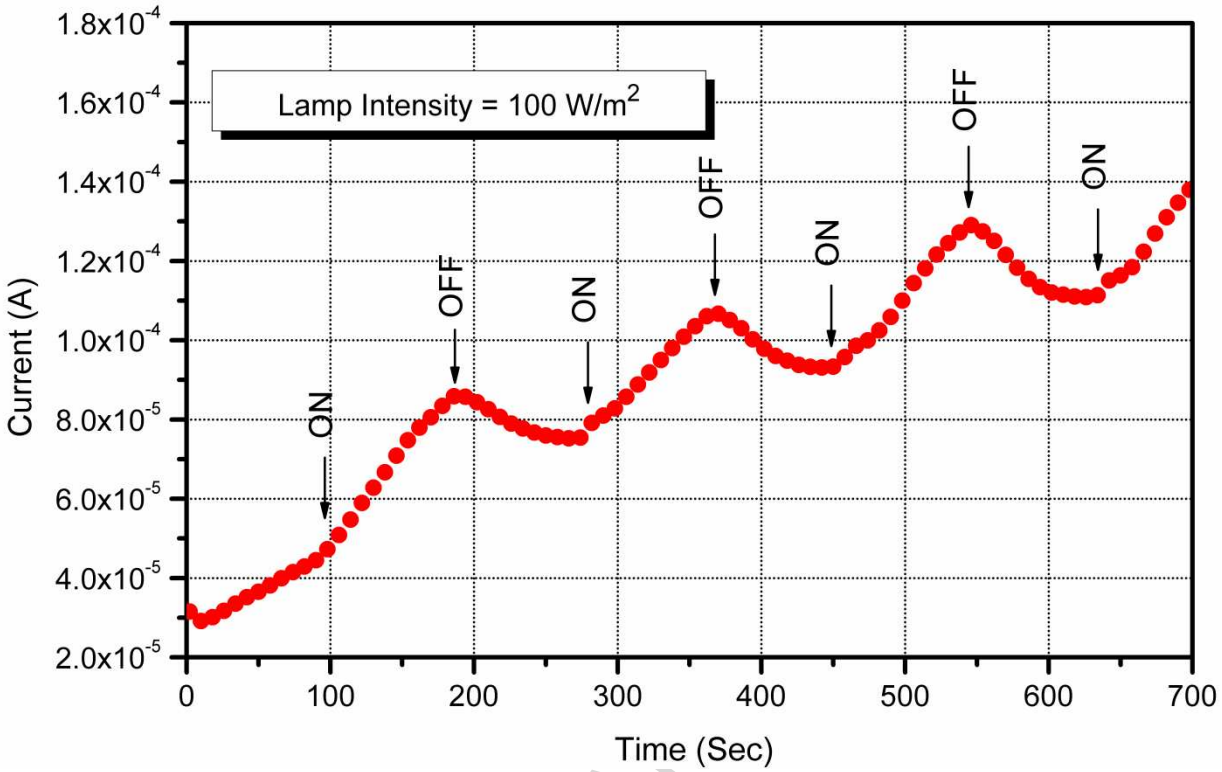

Figure 10: Sachin Rondiya et al.

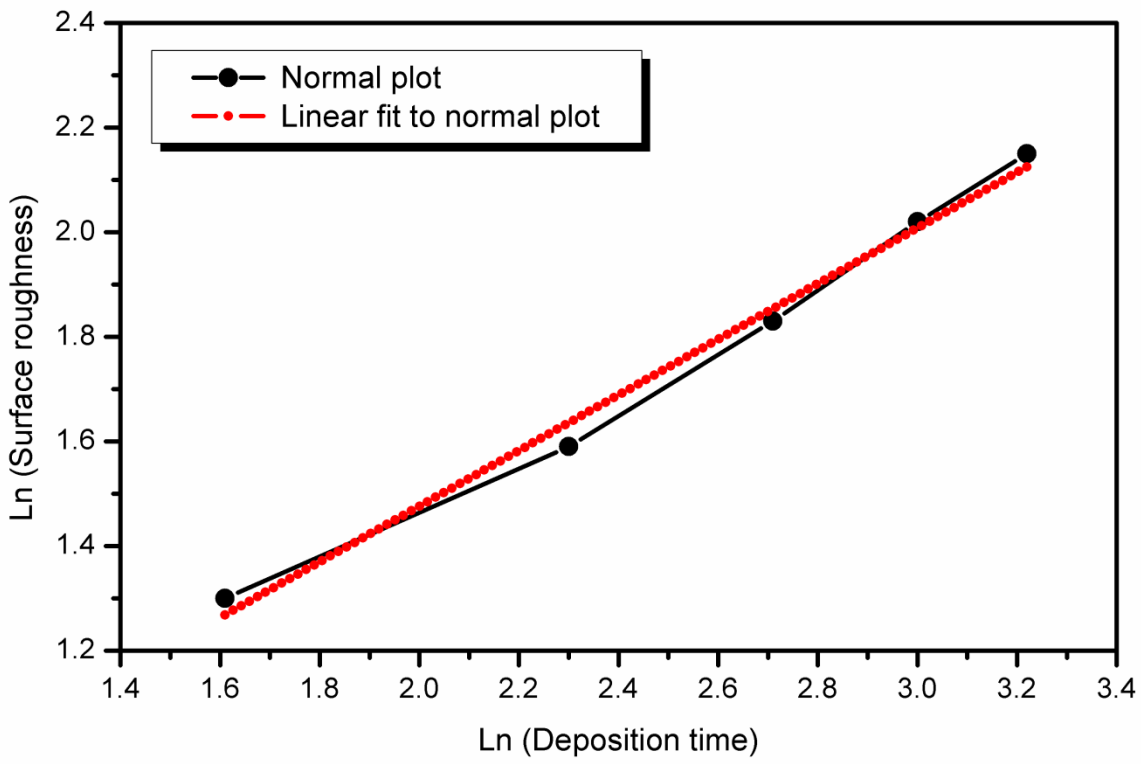

Figure 11: Sachin Rondiya et al.

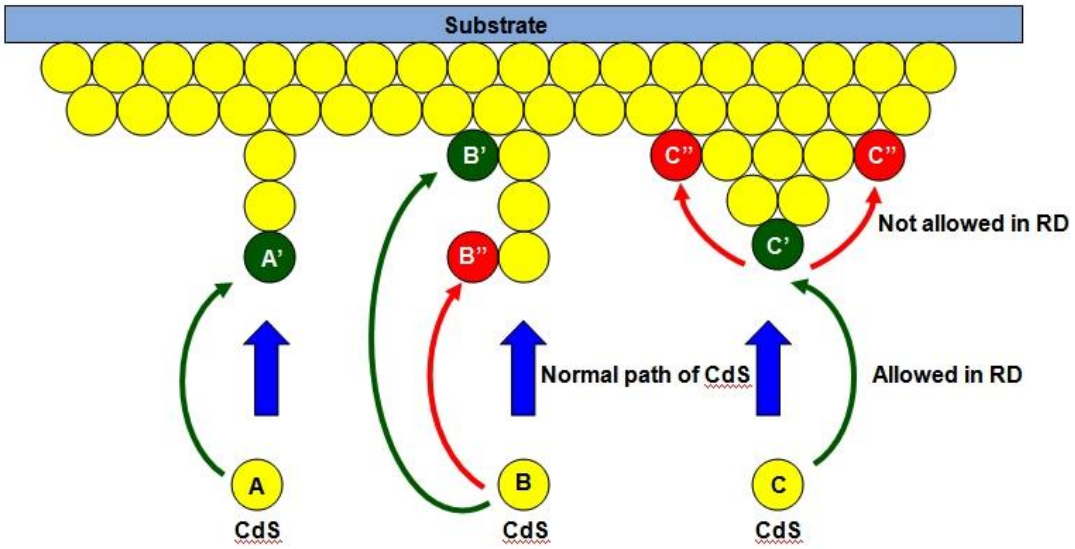

Figure 12: Sachin Rondiya et al.

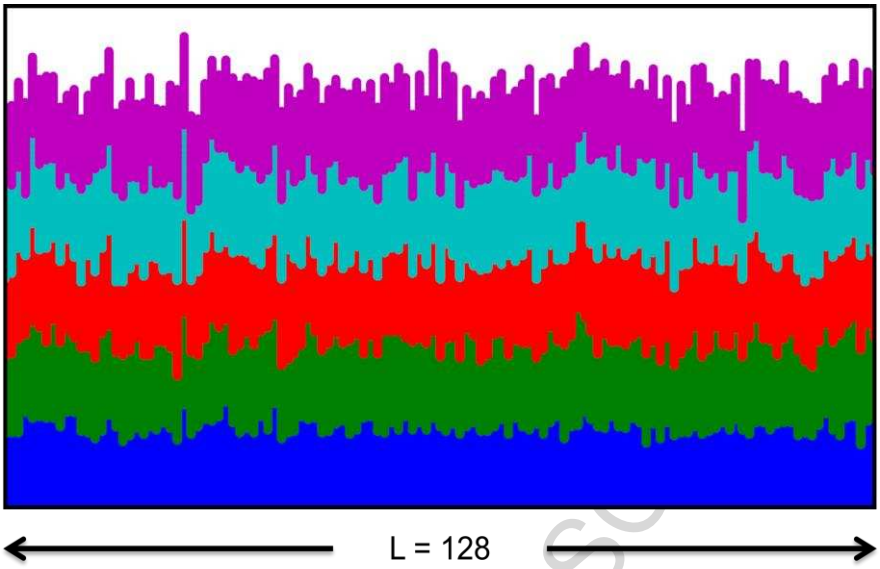

HIGHLIGHTS OF MANUSCRIPT:

- Synthesis of CdS thin films at room temperature by RF sputtering at various deposition time
- Formation of CdS thin films has been confirmed by XRD, Raman spectroscopy, XPS, TEM
- Formation of nearly stoichiometric CdS films
- Photodetector fabricated using RF sputtered CdS film show an excellent photo-response
- Experimental uncorrelated growth of CdS films is validated by Monte-Carlo simulation